Supplement of Atmos. Chem. Phys., 17, 13119–13138, 2017
https://doi.org/10.5194/acp-17-13119-2017-supplement

Atmospheric Chemistry and Physics
Open Access
EGU

Supplement of

Frequent ultrafine particle formation and growth in Canadian Arctic marine and coastal environments

Douglas B. Collins et al.

Correspondence to: Douglas B. Collins (douglas.collins@utoronto.ca)

1 Air Mass Histories

In the main text, air mass histories were provided based on FLEXPART model results for various release times that coincide with ultrafine particle (UFP) formation and growth events. As seen in Figure 3, $N_{4\text{-}20}$ concentrations were greater than 1000 cm^{-3} at and around Pond Inlet. These were not enclosed in a box due to the lack of apparent growth in the size distributions measured in this region. In addition, as shown in Figure S1, the 5-day potential emission sensitivities show strong influence from terrestrial northern Canada and Alaska, which supports the notion that UFP formation and growth in the Canadian Arctic was associated with marine and/or coastal influences.

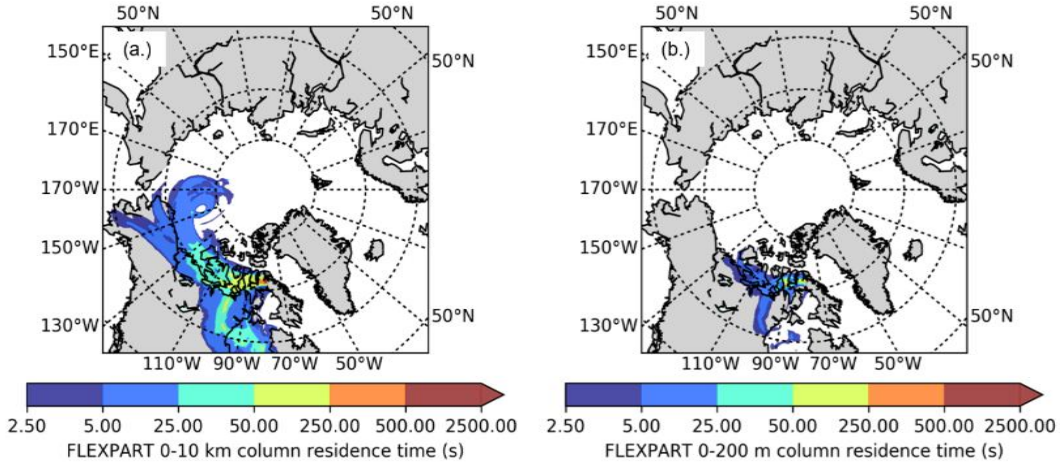

Figure S1: Air mass history extending 5 days backward from 3 August 2016 18:00 UTC, when the ship was located near Pond Inlet generated by the FLEXPART model. (a.) Time-integrated model results in a 0-10km column and (b.) in a 0-200 m column.

2 Correlations of Particle Growth Rate with Other Measured Parameters

Apparent growth rates of particles were measured for 22 different time periods aboard CCGS *Amundsen* in 2014 and 2016, combined. As described briefly in the main text, some growth events showed a slowing of the apparent (linear) growth rate over time, as particles grew larger. In cases where this was clearly occurring, the events were split into sub-events to show the true growth characteristics. Figure S2 shows, however, that a correlation between particle size and growth rate was not universally observed. Inspection of the apparent growth rate as a function of particle size shows that higher growth rates, when observed, tended to be associated more often with smaller particle sizes, although slow growth was also observed in particles of small size (d_p < 40 nm). Extremely high growth rates (GR_{app} > 10 nm h^{-1}, open circles in Figure S2) were segregated in the correlation analysis provided in Figures S2 and S3 to indicate how correlations change when these cases are excluded.

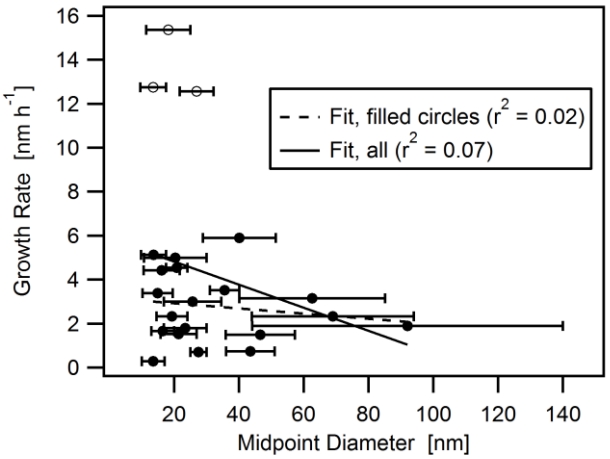

Figure S2: Apparent growth rate of particles compared with the midpoint of the diameter interval in which growth was measured. The markers indicate the midpoint, with the bars showing the diameter growth intervals. The dashed line is a linear least squares fit to the solid filled circles and the solid line is a linear least squares fit to all points.

To assess the potential influence of certain environmental parameters on particle growth, the growth rate was correlated with mean solar radiation, daily maximum solar radiation, and the total condensation sink (Figure S3). A moderate correlation existed between solar radiation and apparent growth rate when the rates greater than 10 nm h^{-1} were excluded (considering filled circles only); correlation was poorer when including all points. Neither the maximum solar radiation observed on the day in which formation/growth was initiated nor the condensation sink (CS) were correlated with the apparent growth rate.

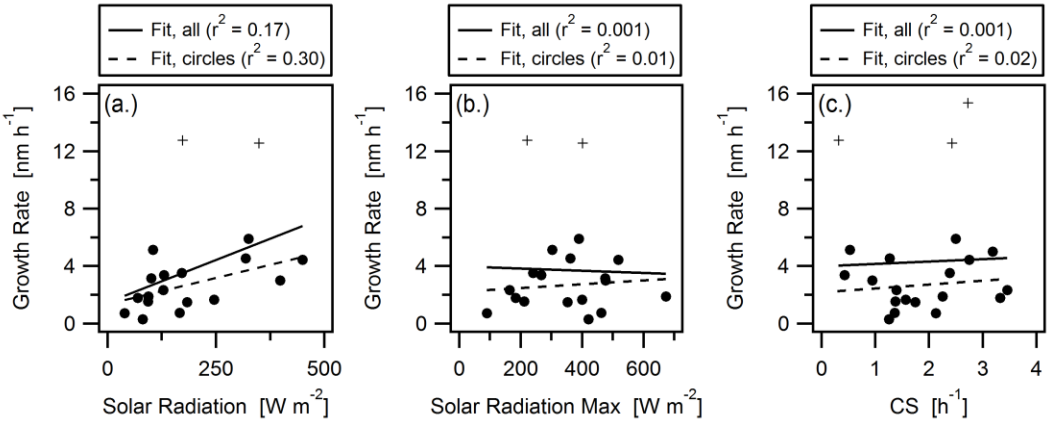

Figure S3: Correlations of measured apparent particle growth rates with (a.) mean solar radiation measured during the same time interval as the growth rate, (b.) solar radiation maximum for the day on which the UFP formation/growth event occurred, and (c.) the mean condensation sink (CS) measured during the time interval in which growth rate was measured. The dashed lines are linear least squares fits to the solid circles, and the solid lines are linear least squares fits to both solid circles and crosses. Crosses correspond with open circles in Figure S2.

3 Satellite Data Analysis

Maps of MODIS-Aqua liquid cloud fraction are presented in the main text, showing spatial differences in monthly average cloud fraction. Statistical analysis of the cloud fraction indicates small overall differences between August 2014 and 2016 within the study area box shown in Figure 10. Histograms of the per-grid box cloud fractions and the per-grid box difference (2016 minus 2014) are given in Figure S4. The average grid box value for cloud fraction within

the study area was approximately 0.3 for both years. The average difference (2016 minus 2014) was approximately 0.001, which is well within the uncertainty of the measurements. These bulk statistical values clearly indicate that the study region was, on average, similarly cloudy during both expeditions (Figure S4a), although the spatial distribution of cloudiness was different, as evidenced by the width of the frequency distribution in Figure S4b and the image in Figure 10c.

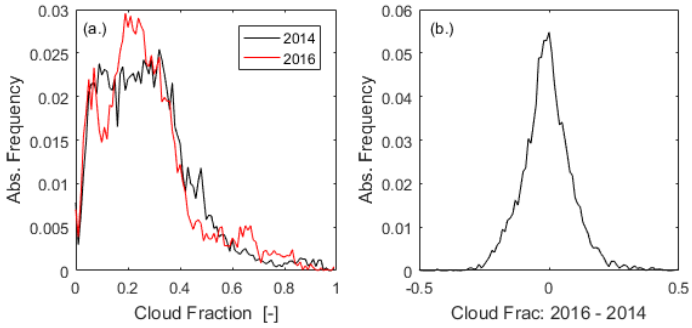

Figure S4: Frequency distributions of (a.) cloud fraction values from 2014 and 2016 and (b.) per-grid square difference in cloud fraction between 2016 and 2014.

A basic analysis of sea ice conditions is presented in the manuscript, showing lower sea ice concentrations in 2016 relative to 2014. Example images are shown from 1 August 2014 and 2016, with a difference map for that day. To indicate the differences in sea ice concentration throughout the study period, the daily average of sea ice fraction differences (2016 minus 2014) calculated from daily satellite retrievals are shown in Figure 12. Differences were calculated for each spatial grid element, and the difference values were averaged for each daily data set. A steep change in sea ice fraction difference was observed at the end of July, with relative differences in sea ice more pronounced throughout August. Figure 12 also shows the normalized (or relative) differences in sea ice concentration, which were referred to in Section 3.3.2 in the main text, calculated using Eq. S1:

$$Relative\ Difference = \frac{(\sum_{i=1}^{n}(SI_{2016,i} - SI_{2014,i}))/n}{\overline{SI_{2014}}} \qquad \text{(S1)}$$

where $SI_{2014,i}$ and $SI_{2016,i}$ are sea ice concentrations on the i^{th} element of total number of elements, n, in the spatial grid throughout which the satellite retrieval product was analysed in this study, and $\overline{SI_{2014}}$ represents the average sea ice concentration for the study period in 2014.

4 Nitrate Profiles in the Ocean

Nitrate concentrations in seawater were obtained at a number of stations throughout each expedition. To aid in understanding differences between the 2014 and 2016 expeditions, depth profiles from the surface to 200 meters have been grouped by location in Figure S5. The relative difference between the 2014 and 2016 nitrate profiles has been provided in Figure S5e. Deviations to negative values between the surface and 30 m depth suggest that in each region, except Baffin Bay, nitrate concentrations were lower in 2016. The analysis in Baffin Bay is hampered by containing data from only 3 stations in 2014, which could lead to the behaviour shown in Figure S5e, where the normalized differences became very high (approx. 1600%) at 20 m depth and all stations at 0 m depth were fully depleted in nitrate in both years. In other locations, even when a large proportion of surface stations had low concentrations (including those below the detection limit), some stations showed appreciable concentrations, so average values were larger than zero.

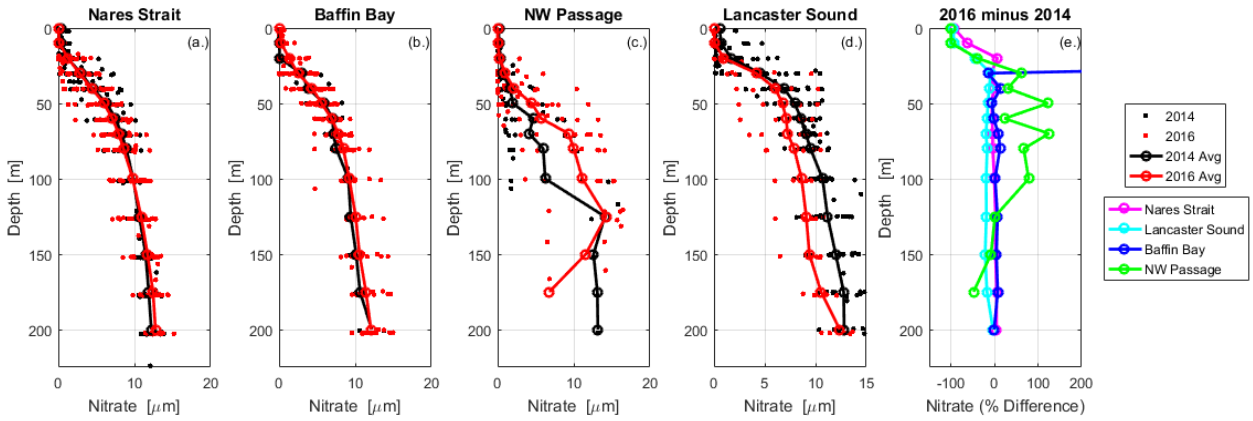

Figure S5: Profiles of nitrate in seawater separated by region and by year. Small dots represent individual measurements and thick open circles denote depth-resolved average concentrations. The panel on the right shows % difference in nitrate profile concentrations.